[Fe II (TRIM) 2]F 2 , the First Example of Spin Conversion Monitored by Molecular Vibrations

ARTICLE *in* INORGANIC CHEMISTRY · FEBRUARY 1996

Impact Factor: 4.76 · DOI: 10.1021/ic9506567 · Source: PubMed

6 AUTHORS, INCLUDING:

M. Verelst
Centre d'Élaboration de Matériaux et d'Etud…
88 PUBLICATIONS **2,293** CITATIONS
SEE PROFILE

Gilles Lemercier
Université de Reims Champagne-Ardenne
75 PUBLICATIONS **798** CITATIONS
SEE PROFILE

$[Fe^{II}(TRIM)_2]F_2$, the First Example of Spin Conversion Monitored by Molecular Vibrations

Azzedine Bousseksou,[†] Marc Verelst,[†] Hector Constant-Machado,[‡] Gilles Lemercier,[†] Jean-Pierre Tuchagues,*[,†] and François Varret[‡]

Laboratoire de Chimie de Coordination du CNRS, UP 8241 liée par conventions à l'Université Paul Sabatier et à l'Institut National Polytechnique, 205 route de Narbonne, 31077 Toulouse Cedex, France, and Laboratoire Optique et Magnétisme, CNRS, URA 1531, Université de Versailles, 45 avenue des Etats Unis, 78035 Versailles Cedex, France

Received May 30, 1995[⊗]

The new $[Fe^{II}(TRIM)_2]F_2$ spin-crossover complex (TRIM = 4-(4-imidazolylmethyl)-2-(2-imidazolylmethyl)-imidazole) has been synthesized, crystallizing in the monoclinic system, space group $P2/n$, with $Z = 2$, $a = 9.798(2)$ Å, $b = 8.433(2)$ Å, $c = 14.597(3)$ Å, and $\beta = 90.46(1)°$. The structure was solved by direct methods and refined to conventional agreement indices $R = 0.032$ and $R_w = 0.034$ with 1378 unique reflections for which $I > 3\sigma(I)$. The molecular structure consists of $[Fe(TRIM)_2]^{2+}$ complex cations hydrogen-bonded to six fluoride anions. The crystal packing results from this highly symmetrical and dense 3D network of hydrogen bonds. The coordination geometry of the iron(II) center can be described as a weakly distorted octahedron, including six nitrogen atoms originating from the two TRIM ligands coordinated to Fe(II) through their imine nitrogen atoms. Investigation of $[Fe^{II}(TRIM)_2]F_2$ by magnetic susceptibility measurements and Mössbauer spectroscopy as a function of temperature indicates a 5% thermal variation of the spin fraction between 50 and 150 K, at variance with all previous litterature data. The spin conversion is gradual with 6% LS fraction below 50 K and less than 1% above 150 K. A theoretical approach based on the Ising-like model, completed with harmonic oscillators associated with the 15 vibration modes of the FeN_6 coordination octahedron, successfully fits the data with an energy gap of ∼40 K between the lowest LS and HS electrovibrational states, an average vibration frequency ω_{LS} of 232 K in the LS state, and an average ω_{LS}/ω_{HS} ratio of 1.3. Taking these results into account, the computed molar entropy change ΔS associated with a complete conversion between the HS and LS states of $Fe^{II}(TRIM)_2F_2$ (∼40 $J\cdot K^{-1}\cdot mol^{-1}$) is in fair agreement with the expected value.

Introduction

The temperature-induced LS ↔ HS ($^1A_1 \leftrightarrow {}^5T_2$) spin-state conversion of Fe^{II} has been extensively studied over the last two decades, and several reviews have summarized the most prominent results.[1] Soraï and Seki have noted the prevailing role of intramolecular vibrations in spin conversions throughout experimental heat capacity studies.[2] However, the experimental conversion curves, $n_{HS}(T)$, where n_{HS} is the fraction of molecules in the HS state, have not yet provided any direct information regarding the role of molecular vibrations.

Due to the vibronic origin of the spin-crossover phenomenon, models based on electron−phonon coupling are in principle the most relevant. They have been developed either in the Debye approximation by Zimmerman and König[3a] or on a Jahn−Teller basis by Kambara.[3b]

In practice, only approximative models have been widely used: thermodynamic models,[4] or their equivalent Ising-like (*i.e.* two-level) models,[5] yielding conversion curves deprived of any specific vibrational effect (in the absence of cooperativity, the mass action law is obeyed, and the Arrhenius plot $\ln(n_{HS}(T)/n_{LS}(T))$ vs $1/T$ is linear as a first approach).

In a recent work,[6] we observed a slight curvature of the Arrhenius plot for $[Fe^{II}(TRIM)_2]Cl_2$, in qualitative agreement with the predictions of a recently introduced simple electrovibrational model,[7] including two-level electronic systems completed by LS or HS harmonic oscillators.

On the basis of the molecular crystal structure and experimental variation of the high-spin fraction with temperature obtained from the magnetic susceptibility and Mössbauer measurements of the new $[Fe^{II}(TRIM)_2]F_2$ spin-crossover complex, we report here the first evidence of a spin-state conversion "entirely" monitored by vibrations and analyzed by using the electrovibrational model presented in ref 7.

Experimental Section

Materials. All reagents were of analytical grade and were used without further purification. Solvents were degassed under vacuum prior to use. Due to the high reactivity of iron(II) salts and complexes with dioxygen, all complexes were prepared under purified nitrogen atmosphere in Schlenk-type vessel or in an inert-atmosphere box (Vacuum Atmospheres HE 43-2) equipped with a Dry-Train (Jahan EVAC 7).

* To whom correspondence should be addressed. Fax: (33) 61 55 30 03. email: tuchague @ lcctou.lcc-toulouse.fr.
[†] Laboratoire de Chimie de Coordination du CNRS.
[‡] Laboratoire Optique et Magnétisme.
[⊗] Abstract published in *Advance ACS Abstracts,* December 1, 1995.

(1) (a) Goodwin, H. A. *Coord. Chem. Rev.* **1976**, *18*, 293. (b) Gütlich, P. *Struct. Bonding* **1981**, *44*, 83. (c) Beattie, J. K. *Adv. Inorg. Chem.* **1988**, *32*, 1. (d) Toftlund, H. *Coord. Chem. Rev.* **1989**, *94*, 67. (e) König, E. *Struct. Bonding* **1991**, *76*, 51.
(2) Soraï, M.; Seki, S. *J. Phys. Chem. Solids* **1974**, *35*, 555.
(3) (a) Zimmermann, R.; König, E. *J. Phys. Chem. Solids* **1977**, *38*, 779. (b) Kambara, T. *J. Chem. Phys.* **1979**, *70*, 4199.
(4) (a) Slichter, C. P.; Drickamer, H. G. *J. Chem. Phys.* **1972**, *56*, 2142. (b) Purcell, K. F.; Edwards, M. P. *Inorg. Chem.* **1984**, *23*, 2620. (c) Spiering, H.; Meissner, E.; Köppen, H.; Müller, E. W.; Gütlich, P. *Chem. Phys.* **1982**, *68*, 65. (d) Bousseksou, A., Ph.D. Thesis, University of Paris VI, France, 1992.
(5) (a) Bari, R. A.; Sivardière, J. *J. Phys. Rev.* **1972**, *B5*, 4466. (b) Wajnflasz, J. *J. Phys. Stat. Solids* **1970**, *40*, 537. (c) Bousseksou, A.; Nasser, J.; Linares, J.; Boukheddaden, K.; Varret, F. *J. Phys. I (Paris)* **1992**, *2*, 1381. (d) Bousseksou, A.; Nasser, J.; Linares, J.; Boukheddaden, K.; Varret, F. *Mol. Cryst. Liq. Cryst.* **1993**, *234*, 269.
(6) Lemercier, G.; Bousseksou, A.; Verelst, M.; Tuchagues, J.-P.; Varret, F. *J. Magn. Magn. Mater.* **1995**, *150*, 227.
(7) Bousseksou, A.; Constant-Machado, H.; Varret, F. *J. Phys. I (Paris)* **1995**, *5*, 747.

0020-1669/96/1335-0110$12.00/0

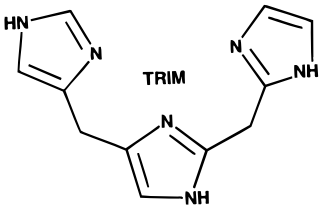

Figure 1. Schematic representation of 4-(4-imidazolylmethyl)-2-(2-imidazolylmethyl)imidazole, abbreviated TRIM.

Ligand. The triimidazole ligand (4-(4-imidazolylmethyl)-2-(2-imidazolylmethyl)imidazole)) abbreviated TRIM throughout the paper (Figure 1) has been synthesized as a faint-yellow microcrystalline powder by E. Mulliez.[8]

$[Fe^{II}(TRIM)_2]F_2$ (2). White microcrystalline powder samples of **2** were prepared by adding solid ammonium fluoride to a freshly prepared deep purple methanolic solution of $Fe^{II}(TRIM)_2(ClO_4)_2$ (**1**) (2.05:1 stoichiometry) and precipitating **2** by addition of acetonitrile after 4 days of reaction under stirring during which the reaction mixture turned slowly dark blue. The precipitation rate is slow, and 12 h is necessary to obtain a maximum yield of **2** (40%). The slight excess of NH_4F is necessary to avoid coprecipitation of **1**. The deep purple solution of precursor **1** was freshly prepared by dropwise addition of a 5 mL methanolic solution of $Fe^{II}(ClO_4)_2 \cdot 6H_2O$ (446 mg, 1.23 mmol) to a 5 mL methanolic solution of $TRIM \cdot H_2O$ (575 mg, 2.33 mmol). *(Caution: perchlorate salts and complexes are potential explosives and should be handled in small quantities and with much care!).* Single crystals of **2** suitable for X-ray studies were obtained by slow concentration of 2×10^{-3} M methanolic solutions of the complex in an inert-atmosphere box. IR (CsBr, cm^{-1}): 3146−3087, 1419 (ν_{NH_4}); 3023−2493 ($\nu_{NH} + \nu_{CH}$); 1577, 1185 (δ_{NH}(in plane)); 1428 (ν_{Im}); 1325 (Δ'_{Im}); 1124, 1117 (δ_{CH}(Im)); 920, 904 (δ_{CH}(in plane)); 823, 812 (δ_{NH}(out of plane)); 771, 748, 737 (Δ_{Im}); 652, 627 (Γ_{Im}); 479, 384, 285 (ν_{FeN}). Anal. Calcd for $FeC_{22}H_{24}N_{12}F_2$ (**2**): C, 48.0; H, 4.4; N, 30.5; F, 6.9; Fe, 10.1. Found: C, 46.3; H, 4.5; N, 29.9; F, 9.1; Fe, 9.5. The resulting vacuum-dried microcrystalline compound is moderately sensitive to dioxygen.

Physical Mesurements. Elemental analyses were carried out at the Laboratoire de Chimie de Coordination Microanalytical Laboratory in Toulouse for C, H, and N and at the Service Central de Microanalyses du CNRS in Vernaison for F and Fe.

IR spectra were recorded on a Perkin-Elmer 983 spectrophotometer coupled with a Perkin-Elmer infrared data station. Samples were run as CsBr pellets.

TGA measurements were carried out with a SETARAM TG-DTA92 apparatus coupled with a Leybold Heraeus QX 2000 mass spectrometer.

Variable-temperature magnetic susceptibility data were obtained on powdered samples with a Quantum Design MPMS SQUID susceptometer. Diamagnetic corrections were applied by using Pascal's constants.

Mössbauer measurements were obtained on a constant-acceleration conventional spectrometer with a 25 mCi source of ^{57}Co (Rh matrix). Isomer shift values (δ) throughout the paper are given with respect to metallic iron at room temperature. The absorber was a sample of 120 mg of microcrystalline powder enclosed in a 18 mm diameter cylindrical plastic sample holder, the size of which had been determined to optimize the absorption. Variable-temperature spectra were obtained in the 300−4.2 K range, by using an MD 306 Oxford cryostat, the thermal scanning being monitored by an Oxford ITC4 servocontrol device (±0.1 K accuracy). A least-squares computer program[9] was used to fit the Mössbauer parameters and determine their standard deviations of statistical origin (given in parentheses).

All samples used for physical or chemical characterizations were prepared inside a drybox under a purified nitrogen atmosphere. We exercised all necessary care while transferring the samples to prevent any aerial oxidation. In particular, the SQUID and Mössbauer sample holders were sealed with melted paraffin inside the drybox prior to their transfer to the spectrometer and the sample chamber was carefully flushed with purified nitrogen or helium during introduction of the sample.

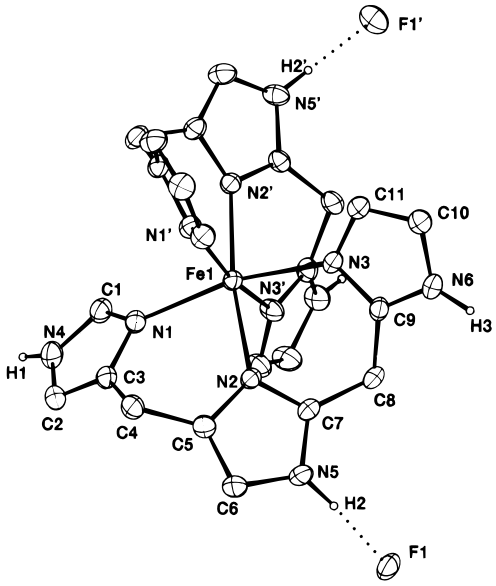

Figure 2. ORTEP view of the $[Fe^{II}(TRIM)_2]F_2$ molecule (**2**) with atom numbering.

X-ray Crystal Structure Determination. A white transparent parallelepiped ($0.30 \times 0.20 \times 0.15$ mm^3) was coated with Vaseline in an inert-atmosphere box and sealed in a Lindemann capillary that was mounted on an Enraf-Nonius CAD4 diffractometer. A total of 2634 reflections with $3° \le 2\theta \le 54°$ were collected at 20 °C using Mo Kα radiation with a graphite monochromator ($\lambda = 0.7107$ Å). The crystal of $[Fe(TRIM)_2]F_2$ belongs to the monoclinic system, and its space group was assigned as $P2/n$ (No. 13). The crystal quality was monitored by scanning three standard reflections every 2 h. No significant variation was observed during the data collection. After corrections for Lorentz and polarization effects, an empirical absorption correction was applied.[10] Cell constants were obtained from a least-squares fit of 25 reflections.

Structure Solution and Refinement. The structure was solved by using direct methods.[11] With a final data set of 1378 reflections ($I > 3\sigma(I)$), all non-hydrogen atoms were located in successive Fourier difference maps and least-squares refinement cycles.[12] The NH hydrogen atoms of the TRIM ligand were found on a difference Fourier synthesis and refined while the other were included in calculations with a constrained geometry (C−H = 0.98 Å). Non-hydrogen atoms were refined anisotropically. NH hydrogen atoms were refined isotropically, and all other hydrogen atoms were coupled to their bonded carbon atoms with isotropic temperature factors 20% higher than those of the respective bonded atoms. The atomic scattering factors and anomalous dispersion terms were taken from the standard compilation.[13] The final full-matrix least-squares refinement converged to $R = 0.032$ and $R_w = 0.034$ with a unit weighting scheme.

All calculations were performed on a PC computer using the programs SHELXS 86[11] and CRYSTALS.[12] The $[Fe(TRIM)_2]F_2$ complex molecule is shown in Figure 2 with atom numbering. The crystallographic data are summarized in Table 1, and final fractional atomic coordinates and selected bond lengths and bond angles with esd's are given in Tables 2 and 3, respectively. Complete crystallographic data have been deposited.[14]

(8) Mulliez, E. *Tetrahedron Lett.* **1989**, *30*, 6169.
(9) Varret, F. *Proceedings of the International Conference on Mössbauer Effect Applications*, Jaipur, India, 1981; Indian National Science Academy: New Delhi, 1982.
(10) Walker, N.; Stuart, D. *Acta Crystallogr., Sect. A: Found. Crystallogr.* **1983**, *A39*, 158.
(11) Sheldrick, G. M. *SHELXS 86: Program for Crystal Structure Solution*, University of Göttingen: Göttingen, Germany, 1986.
(12) Watkin, D. J.; Carruthers, J. R.; Betteridge, P. W. *CRYSTALS: Advanced Crystallographic Program System*; Oxford University: Oxford, U.K., 1988.
(13) Cromer, D. T.; Waber, J. T. *International Tables for X-ray Crystallography*; Kynoch Press: Birmingham, U.K., 1974; Vol. IV.

Table 1. Crystallographic Data for $[Fe^{II}(TRIM)_2]F_2$ (**2**)

empirical formula: $FeC_{22}H_{24}N_{12}F_2$	fw: 550
space group: *P*2/*n* (No. 13)	$T = 20$ °C
$a = 9.798(2)$ Å	$\alpha = 90.00(2)°$
$b = 8.433(2)$ Å	$\beta = 90.46(1)°$
$c = 14.597(3)$ Å	$\gamma = 90.00(1)°$
$V = 1206(1)$ Å^3	$\lambda = 0.7107$ Å
$\rho_{calc} = 1.52$ g cm^{-3}	μ(Mo Kα) = 6.75 cm^{-1}
$Z = 2$	transm coeff = 0.961−1.0
R ($\sum\|\|F_o\| - \|F_c\|\|$)/ ($\sum\|F_o\|$) = 0.032	R_w ($[\sum(\|F_o\| - \|F_c\|)^2$/ $(\sum\|F_o\|)^2]^{1/2}$) = 0.034

Table 2. Fractional Atomic Coordinates (Esd's) and Isotropic Equivalent Temperature Factors for $[Fe^{II}(TRIM)_2]F_2$ (**2**)

atom	*x*/*a*	*y*/*b*	*z*/*c*	U_{eq}(Å^2)[a]
Fe	0.2500	0.01650(8)	0.7500	0.0263
F	0.3303(2)	0.3987(3)	0.3637(1)	0.0435
N(1)	0.1123(3)	−0.1634(3)	0.6947(2)	0.0325
N(2)	0.3188(3)	0.0378(3)	0.6090(2)	0.0295
N(3)	0.4074(3)	0.1967(3)	0.7713(2)	0.0328
N(4)	−0.0801(3)	−0.2815(4)	0.6577(2)	0.0411
N(5)	0.3453(3)	0.1609(4)	0.4782(2)	0.0360
N(6)	0.5536(3)	0.3828(4)	0.7350(2)	0.0377
C(1)	−0.0149(4)	−0.1915(4)	0.7187(2)	0.0374
C(2)	0.0102(4)	−0.3133(4)	0.5896(3)	0.0404
C(3)	0.1288(4)	−0.2417(4)	0.6123(2)	0.0333
C(4)	0.2602(4)	−0.2358(4)	0.5613(2)	0.0372
C(5)	0.2983(3)	−0.0686(4)	0.5390(2)	0.0320
C(6)	0.3142(4)	0.0062(5)	0.4581(2)	0.0402
C(7)	0.3468(3)	0.1752(4)	0.5698(2)	0.0298
C(8)	0.3722(4)	0.3270(4)	0.6191(2)	0.0347
C(9)	0.4429(4)	0.3013(4)	0.7085(2)	0.0315
C(10)	0.5911(4)	0.3280(5)	0.8192(3)	0.0444
C(11)	0.5017(4)	0.2128(4)	0.8409(3)	0.0385
H(1)	−0.164(3)	−0.316(4)	0.659(2)	0.05(1)*
H(2)	0.352(4)	0.244(5)	0.439(2)	0.06(1)*
H(3)	0.590(4)	0.462(5)	0.702(3)	0.07(1)*

[a] U_{eq} is defined as one-third the trace of the orthogonalized $\mathbf{U}_{ij}$ tensor. Starred values indicate that the atoms were refined isotropically.

Table 3. Selected Interatomic Distances (Å) and Angles (deg) for $[Fe^{II}(TRIM)_2]F_2$ (**2**)

		Iron Environment	
		Distances	
Fe−N(1)	2.180(3)	Fe−N(2)	2.178(3)
Fe−N(3)	2.186(3)		
		Angles	
N(1)−Fe−N(2)	84.4(1)	N(1)−Fe−N(3′)	89.8(1)
N(1)−Fe−N(2′)	102.2(1)	N(1)−Fe−N(1′)	91.8(1)
N(2)−Fe−N(3)	81.6(1)	N(2)−Fe−N(2′)	170.5(1)
N(2)−Fe−N(3′)	91.8(1)	N(3)−Fe−N(3′)	91.9(1)
N(1)−Fe−N(3)	166.0(1)		
		Hydrogen Bonds	
		Distances	
N(4)−H(1)	0.88(4)	H(1)···F″	1.81(4)
N(5)−H(2)	0.91(4)	H(2)···F	1.72(4)
N(6)−H(3)	0.90(4)	H(3)···F‴	1.71(4)
		Angles	
N(4)−H(1)−F″	166.9	N(5)−H(2)−F	168.8
N(6)−H(3)−F‴	174.8		

[a] Symmetries: ′ = $^1/_2 - x, y, ^1/_2 - z$; ″ = $-x, -y, 1 - z$; ‴ = $1 - x, 1 - y, 1 - z$.

Results

Synthesis and Compositional Studies. The analytical results and IR spectrum lead to the formulation of complex **2** without any solvent molecule. Compared to the theoretical values, the slightly low percent C and Fe and high percent F indicate that a small amount of ammonium fluoride has coprecipitated with the complex. The proportion of NH_4F evaluated by TGA is approximately 3.5% by weight, in agreement with the analytical results. The numerous metathesis reactions carried out with different **1**:NH_4F stoichiometries indicate that a slight excess of NH_4F is required to avoid coprecipitation of **1** and **2**.

(14) See Supporting Information.

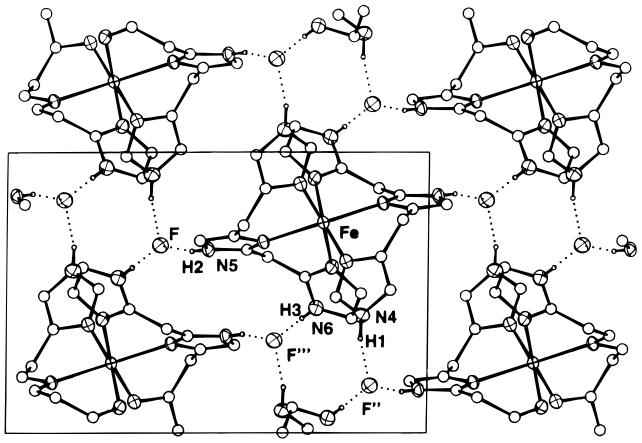

Figure 3. ORTEP view of the unit cell of $[Fe^{II}(TRIM)_2]F_2$ (**2**) projected along *b*.

Molecular Structure of $[Fe(TRIM)_2]F_2$ (2). The structure consists of $[Fe(TRIM)_2]^{2+}$ complex cations hydrogen-bonded to fluoride anions (Figure 2). The coordination geometry of the iron(II) center can be described as a weakly distorted octahedron, including six nitrogen atoms originating from the two TRIM ligands coordinated to Fe(II) through their imine nitrogen atoms. Considering the small range of iron−nitrogen distances (2.178(3)−2.186(3) Å, Table 3), the distortion of the FeN_6 coordination octahedron results from the small N(1)−Fe−N(2) and N(2)−Fe−N(3) bite angles imposed by the TRIM ligand (84.4(1) and 81.6(1)°, respectively). Examination of the least-squares coordination planes, deviations of atoms therefrom, and dihedral angles between coordination planes[14] confirms the presence of a slight rhombic distortion of the FeN_6 coordination octahedron in **2**.

Each $[Fe(TRIM)_2]^{2+}$ complex cation is connected to six fluoride anions through strong N−H···F hydrogen bonds with N···F distances ranging from 2.605(3) to 2.659(4) Å, and reciprocally each fluoride anion is connected to three complex cations (Table 3 and Figure 3). The crystal packing afforded by this highly symmetrical and dense 3D network of hydrogen bonds results in intermetallic distances between adjacent complex cations ranging from 8.433 to 9.798 Å.[14]

Magnetic Susceptibility. The magnetic susceptibility of complex **2** was measured in the 300−2 K temperature range, and the χT versus T curve (Figure 4) shows two inflections located near 120 and 60 K which delineate sections characterized by different slopes. In the 300−120 K section (a) μ_{eff}/Fe is practically constant (5.24−5.16 μ_B); the variation of the magnetic moment is larger in the 120−60 K section (b) (5.16−5.01 μ_B) while μ_{eff}/Fe is again practically constant in the next 60−45 K section (c) (5.01−4.98 μ_B); finally, the 45−2 K low-temperature section (d) is characterized by a significant lowering of the magnetic moment (4.96−2.78 μ_B). The effective magnetic moment per iron at 300 K is larger than the spin-only value of 4.9 μ_B for $S = 2$ as usually observed for high-spin iron(II) complexes. The $^5T_2$ ground state is split by the ligand field and spin−orbit coupling, giving levels separated by energies of the order of kT (thermally populated in the high-temperature range), which results in slightly temperature-

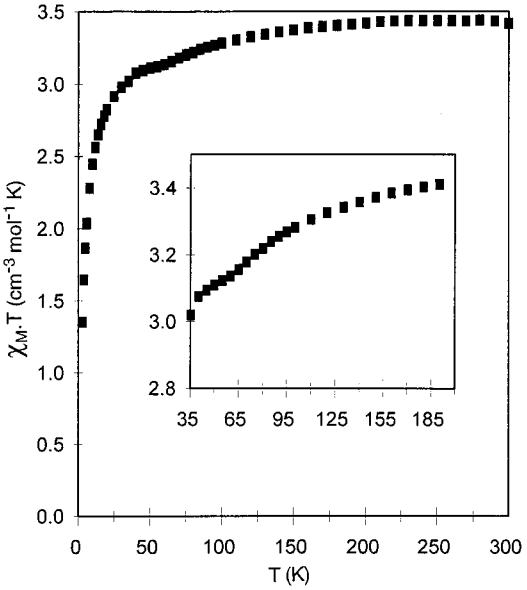

Figure 4. Thermal variation of $\chi_M T$ obtained from magnetic susceptibility measurements of $[Fe^{II}(TRIM)_2]F_2$ (**2**) carried out in the cooling mode.

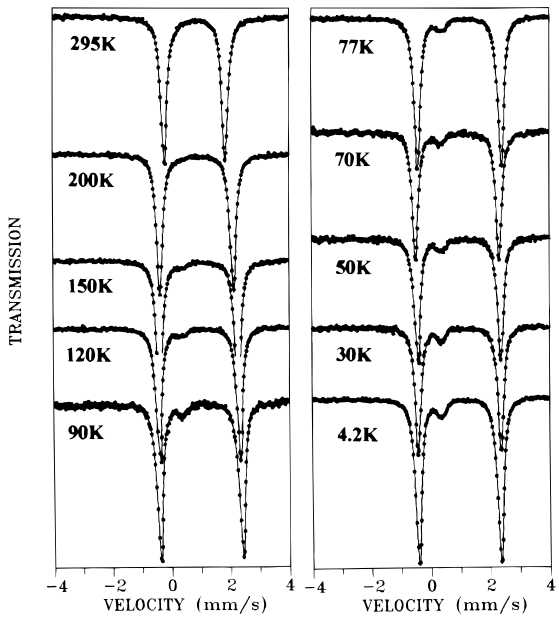

Figure 5. Selected Mössbauer spectra of $[Fe^{II}(TRIM)_2]F_2$ (**2**) obtained in the cooling mode between 295 and 4.2 K. The solid lines represent fitted curves.

dependent magnetic moments above *ca.* 100 K.[15] The very small thermal dependence of μ_{eff}/Fe in section a can be related to this phenomenon. On the other hand, the large thermal dependence of μ_{eff}/Fe in low-temperature section d indicates the presence of zero-field splitting of the high-spin iron(II) ground state and possibly operation of weak intermolecular antiferromagnetic interactions mediated by the highly symmetrical and dense 3D network of hydrogen bonds characterizing this structure. The significant increase in thermal dependence of μ_{eff}/Fe in section b, between 120 and 60 K cannot be related to any previously observed behavior. This unprecedented result has been confirmed by carrying out the magnetic susceptibility measurements several times on the same or different samples, leading to perfectly reproducible results. Finally, it is worth noting that there is a typical reversible (purple-blue ↔ white) color change of complex **2** with temperature between 80 and 100 K, as for most previously studied $Fe(TRIM)_2X_2$ complexes exhibiting the spin-crossover phenomenon.[6,16]

Mössbauer Spectroscopy. Typical Mössbauer spectra are shown in Figure 5, and least-squares-fit parameters are listed in Table 4. A low-spin contribution can be detected at all temperatures, smoothly varying from ~6% (relative area) at 4.2 K to 1% at 295 K. The consistency and physical significance of this small effect were carefully checked: the reversibility of the variation is evidenced by identical spectra recorded at 295 and 77 K before and after the entire set of experiments. Furthermore, as for the magnetic susceptibility measurements, the results were confirmed by carrying out the Mössbauer measurements several times on the same or different samples, leading to perfectly reproducible relative areas (within 1%) and providing thus an additional clue that the low-spin contribution is not due to an impurity.

Table 4. Representative Least-Squares-Fitted Mössbauer Data for $[Fe^{II}(TRIM)_2]F_2$[a,b]

	low-spin state			high-spin state			
T (K)	δ	ΔE_Q	Γ	δ	ΔE_Q	Γ	A_{HS}/A_{tot}
4.2	0.577(6)	0.16(1)	0.25(2)	1.148(4)	2.790(1)	0.246(1)	94.0
50	0.58(1)	0.17(2)	0.25(1)	1.144(1)	2.827(1)	0.246(2)	94.2
77	0.571(8)	0.19(1)	0.25(2)	1.138(1)	2.827(2)	0.244(1)	95.1
150	0.55(2)	*0.23*	0.23(2)	1.111(1)	2.677(1)	0.236(2)	97.8
295	*0.55*	*0.23*	0.23(2)	1.022(1)	2.093(1)	0.246(2)	98.7

[a] δ = isomer shift (mm s^{-1}); ΔE_Q = quadrupole splitting (mm s^{-1}); Γ = width of the lines; A_{HS}/A_{tot} = area ratio of the high-spin doublet to the total area. [b] Statistical standard deviations are given in parentheses. Italic parameters were fixed for the fit.

Discussion

The Mössbauer observation of a LS relative area decreasing on increasing the temperature is a major experimental result. It is interpreted in terms of partial spin-crossover. It is worth considering first the alternative hypothesis that the low-spin contribution may result from the presence of an impurity. Then, the atomic LS and HS fractions should remain constant at all temperatures, although the relative areas might vary a little, due to the Debye−Waller factors of the spin states:[17] the shorter Fe−N bond lengths in the LS state result in larger Debye temperature than in the HS state. Consequently, the relative LS area is expected to slightly increase on increasing temperature. The opposite experimental behavior observed rules out such a possibility. Additionally, when the data are analyzed in terms of spin-crossover, the Debye−Waller correction[17] should remain small and will be neglected here.

It is also important to note that the kinetics of spin conversion become extremely slow at low temperatures.[18] When the system is cooled below a "spin-freezing" temperature (T_f), the spin

(15) Mabbs, F. E.; Machin, D. J. *Magnetic and Transition Metal Complexes*; Chapman and Hall: London, 1973.
(16) (a) Lemercier, G.; Seigneuric, S.; Bousseksou, A.; Varret, F.; Tuchagues, J.-P. *Chem. Phys. Lett.* **1994**, *226*, 289. (b) Lemercier, G.; Mulliez, E.; Brouca-Cabarrecq, C.; Dahan, F.; Bousseksou, A.; Tuchagues, J.-P. Presented at the 30th International Conference on Coordination Chemistry, Kyoto, Japan, July 24−29, 1994. See p 352 of the Proceedings. (c) Lemercier, G. Doctoral Thesis, Université Toulouse III, 1994.
(17) (a) Boukheddaden, K.; Varret, F. *Hyperfine Interact.* **1992**, *72*, 349. (b) Claude, R.; Real, J. A.; Zarembowitch, J.; Kahn, O.; Ouahab, L.; Grandjean, D.; Boukheddaden, K.; Varret, F.; Dworkin, A. *Inorg. Chem.* **1990**, *29*, 4442. (c) König, E.; Ritter, G.; Goodwin, H. A. *Chem. Phys.* **1973**, *1*, 17.
(18) (a) Gütlich, P. *Nucl. Instrum. Methods Phys. Res.* **1993**, *B76*, 387. (b) Hinek, R.; Gütlich, P.; Hauser, A. *Inorg. Chem.* **1994**, *33*, 567.
(19) Takemoto, J. H.; Hutchinson, B. *Inorg. Nucl. Chem. Lett.* **1972**, *8*, 769.

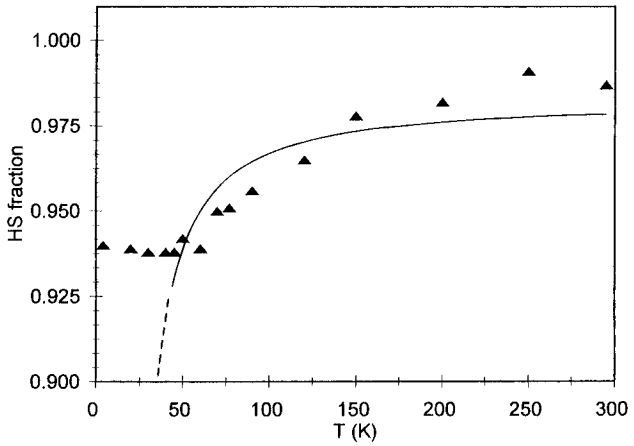

Figure 6. Experimental temperature dependence of the HS fraction (n_{HS}) for $[Fe^{II}(TRIM)_2]F_2$. The solid line represents the best fit obtained with the "two-state" model.

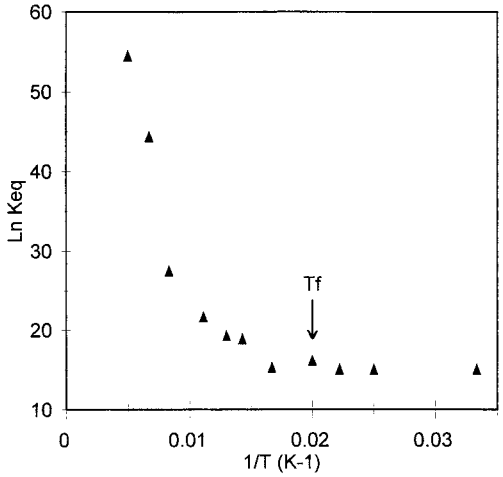

Figure 7. Arrhenius plot of the conversion data for $[Fe^{II}(TRIM)_2]F_2$ (**2**).

equilibrium is no longer reached within the experimental time and the system retains a constant HS fraction. The data in Table 3 lead to $T_f \sim 50$ K, in agreement with literature data originating from kinetic studies of the spin conversion in well-documented cases.[18]

The spin-crossover behavior of the system was elucidated through the following successive steps. (a) The dominating low-temperature HS state clearly suggests that the ground state of the system is HS. Consequently, according to the simple, well-recognized model of Slichter and Drickamer,[4] or its "Ising-type" microscopic equivalent,[5] the HS fraction should slightly decrease on increasing temperature, due to population of the LS state. (b) All attempts at reproducing the experimental trend by using literature models,[4,5] as shown in Figure 6, require the assumption of a LS ground state. Then, the curvature of the computed curve is reversed with respect to the experimental data. This departure cannot be explained by cooperativity which obviously plays a minor role here due to the extremely small variation of spin populations. Such a departure is even better visualized (Figure 7) using an Arrhenius plot: the positive curvature exhibited here is typical for vibrational effects, according to the detailed analysis reported in ref 7. It is worth noting that a similar shape of the conversion curve was presented in the theoretical paper of Zimmerman and König[3] in the particular case of almost equienergetic LS and HS states. (c) The model used here is based on the variations in the molecular vibration frequencies upon spin conversion.[7] Due to the changes in Fe−ligand bond lengths, the fifteen distortion modes of the $Fe^{II}N_6$ octahedron

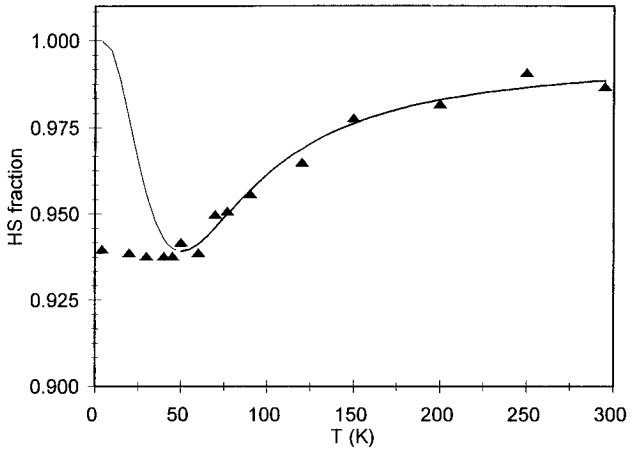

Figure 8. Least-squares fit of the conversion data for **2** to the electrovibrational model. The solid line shows the equilibrium domain where the fit to eq 1 was performed.

differ sizably from the LS to the HS state. Literature data[1e] show that the six Fe−N stretching modes change from LS to HS by a ratio of ~2 to 2.5. The remaining nine modes of lower frequencies have not been identified.

To begin our calculation, an electron vibration Hamiltonian neglecting cooperative interactions is written in the adiabatic (and harmonic) approximation

$$\hat{H} = {}^1/_2\Delta\hat{\sigma} + \sum_{i=1}^{15}(n_i + {}^1/_2)\hbar\omega_i$$

where Δ is the electronic energy gap of the two-level system, σ a fictitious spin taking the values +1 and −1 in the HS and LS states, respectively, n_i the number of vibrational quanta of the ith vibration mode, and ω_i the corresponding frequency, characterized by different values in the LS and HS states.

The electronic degeneracies take the spin-only values (5 and 1 for the HS and LS states, respectively), since the orbital degeneracy of the $^5T_{2g}$ state is lifted by the low-symmetry components of the ligand field, as evidenced by the large value for the quadrupole splitting of the Mössbauer spectra.

For simplicity, we have averaged the fifteen octahedron distortion modes, assuming a single frequency in each spin state. The least-squares fitting of the high-temperature range of the conversion curve (>50 K) leads to an excellent agreement with the data, as shown by Figure 8. The fitted values for the parameters are

$$\Delta = 356 \text{ K}, \quad \omega_{LS} = 232 \text{ K}, \quad \omega_{LS}/\omega_{HS} = 1.297$$

As expected, these values lead to a HS ground state. However, it is worth noting that this result cannot be checked directly by any low-temperature experiment, due to the extremely slow kinetics of the system. A schematic representation of the energy levels is drawn in Figure 9, in order to visualize the effect of thermal population: at low-temperature, the progressive population of the first excited level, which belongs to the LS subspace, results in an increase of the LS (equilibrium) fraction. This initial regime ends near $T \sim 50$ K when the first two levels separated by ~43 K only become nearly equipopulated. A further increase in temperature, involving vibrational excited states, yields an increase of the HS fraction because of the higher density of the vibrational HS states.

Interestingly, the fortuitous coincidence between the minimum of the $n_{HS}(T)$ equilibrium curve and the freezing temperature makes the system only very slightly sensitive to the experimental

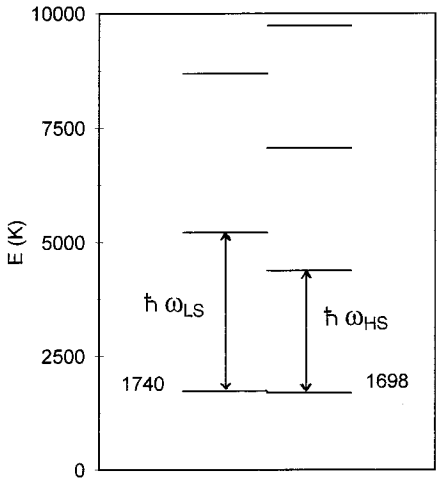

Figure 9. Lower levels of the electrovibrational energy scheme deduced from the fitted parameters for $[Fe^{II}(TRIM)_2]F_2$ (**2**).

cooling rates. Indeed, experiments performed by quenching the sample at 4.2 K and by slowly cooling down (typically decreasing T by 5 K every 6 h) did not induce any difference, at variance with similar experiments reported in the literature.[20] This results from the fact that the equilibrium spin fractions remain nearly the same in the entire temperature range where the conversion rate varies through the accessible range of cooling rates.

The physical relevance of the present analysis is supported by the following conclusive remarks: (i) the fitted value of the average ratio $\omega_{LS}/\omega_{HS} \sim 1.3$ is reasonably smaller than the values reported for the stretching modes (2−2.5) which can be considered as the most sensitive to the spin conversion; (ii) we have computed the molar entropy change ΔS associated with a complete conversion which is merely the vibration + spin entropy difference between the HS and LS states. The value obtained at 150 K (typical spin transition temperature), 40 $J \cdot K^{-1} \cdot mol^{-1}$, falls in fair agreement with literature data (35−80 $J \cdot K^{-1} \cdot mol^{-1}$).[21] Of course, ΔS cannot be measured directly in the present case; neither can it be deduced from an Arrhenius-type analysis.

The small value, ∼40 K, for the energy difference between the HS and LS lowest states is the reason that the conversion curve is no longer monitored by the electronic gap, thus leading to a thermal variation entirely due to the population of the vibrational levels. It also suggests that the complex should be very sensitive to a small applied pressure. This prediction will be tested as soon as possible in one of the very few laboratories equipped to carry out this type of study.

Acknowledgment. E. Mulliez and J. Zarembowitch are gratefully acknowledged, the former for preparing the ligand and the latter for stimulating discussions.

Supporting Information Available: Listings of complete crystal data and experimental details, components of the anisotropic temperature factors, hydrogen atomic positional and thermal parameters, bond lengths and angles, and least-squares planes and deviations of atoms therefrom for complex **2** (7 pages). Ordering information is given on any current masthead page.

IC9506567

(20) Martin, J. P.; Zarembowitch, J.; Bousseksou, A.; Dworkin, A.; Haasnoot, J. G.; Varret, F. *Inorg. Chem.* **1994**, *33*, 6325.
(21) Real, J. A.; Bolvin, H.; Bousseksou, A.; Dworkin, A.; Kahn, O.; Varret, F.; Zarembowitch, J. *J. Am. Chem. Soc.* **1992**, *114*, 4650 and references therein.